Received: 20 January 2022 | Accepted: 24 July 2022

DOI: 10.1111/arcm.12812

ORIGINAL ARTICLE

An archaeometric study of the Konya basin metallic ware through FTIR and XRD analysis with chemometrics: Central Anatolian Early Bronze Age ceramics

İsmail Tarhan[1] | **Michele Massa**[2] | **Yusuf Tuna**[3] | **Fatma Şahin**[4]

[1]Faculty of Science, Department of Biochemistry, Selçuk University, Konya, Turkey

[2]Mansueto Institute for Urban Innovation, University of Chicago, Chicago, IL, USA

[3]Faculty of Science and Letters, Department of Archaeology, Bilecik Şeyh Edebali University, Bilecik, Turkey

[4]Faculty of Letters, Department of Archaeology, Çukurova University, Adana, Turkey

Correspondence
İsmail Tarhan, Selçuk Üniversitesi, Fen Fakültesi, Biyokimya Bölümü, 42130, Selçuklu. Konya, Turkey.
Email: ismtarhan@gmail.com

Funding information
The authors are grateful to the Selçuk University's Scientific Research Projects Foundation and the Luwian Studies Foundation for financially supporting this study.

Abstract

Fourier-transform infrared, X-ray diffraction and chemometrics were used to characterize the mineralogical composition and firing conditions of 59 Early Bronze Age ceramic sherds from the Konya Plain (Turkey). These include the Konya Basin Metallic Ware (KBMW) and a control group of contemporary local products. The analysis indicates significant differences in mineral inclusions and firing temperatures, with KBMW generally being fired above 800°C and characterized by standardized fabric recipes. Assessed together with other published evidence, these results indicate a high degree of specialization in the production of KBMW ceramic assemblages in central Anatolia during the third millennium BCE.

KEYWORDS

Anatolia, ceramic specialization, chemometrics, early Bronze Age, firing temperature, Fourier-transform infrared, Metallic ware, X-ray diffraction

INTRODUCTION

Konya Basin Metallic Ware (KBMW)

The KBMW is a handmade ceramic production typical of the southern-central Anatolian plateau (Turkey) (Fig. 1) during the mid- to late Early Bronze Age (EBA), *c*.2700–2200 BCE (Friedman, 2000; Hacar, 2017) (cf. supplemental material 1 for a more detailed definition of the ware group).

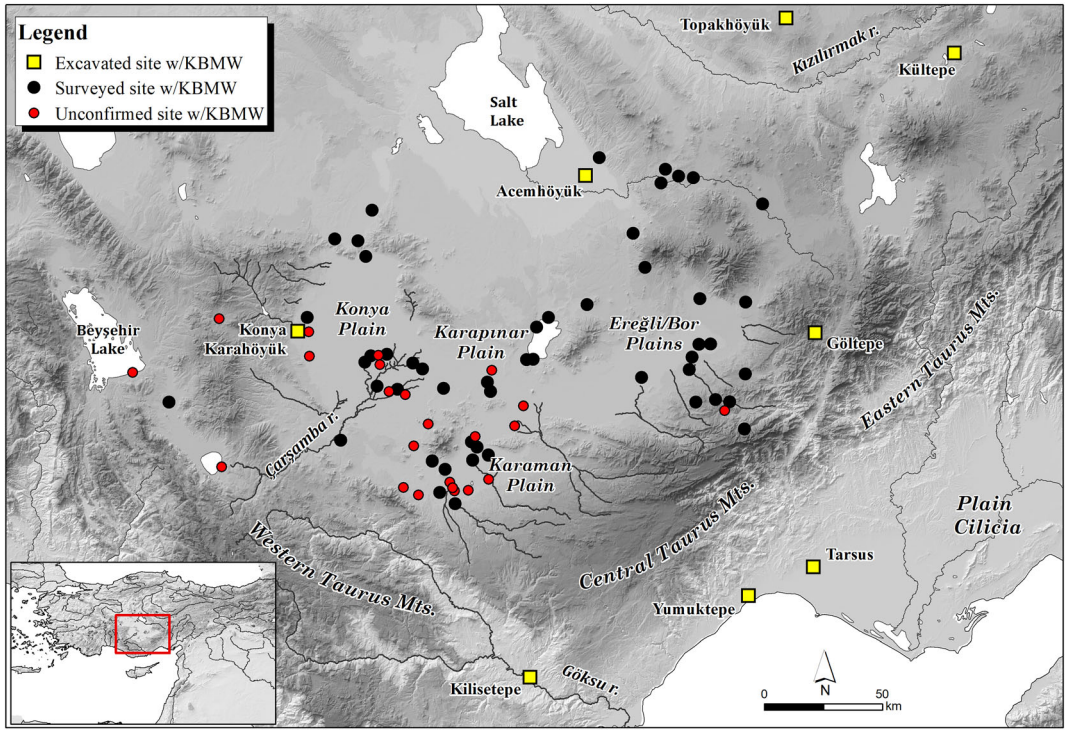

FIGURE 1 Map showing the distribution of known sites with Konya Basin Metallic Ware (KBMW). The inset shows the location of the study area within modern Turkey

The KBMW belong to the broader phenomenon of the Near Eastern 'metallic wares', which were produced between the late fourth and late third millennia BCE (Friedman, 2000; Prub, 2000). Detailed analysis of different metallic wares groups indicate that their ceramic forms are in all cases clearly derived from local contemporary wares, and therefore regional productions are easily distinguishable from one another in morpho-typological terms. The various regional groups, however, have in common several technical traits that set them apart from local wares, such as the exclusive use of mineral temper, dense and thin-walled fabrics, high firing temperatures (at or above 1000°C) and often also reducing firing atmosphere, elements that taken together suggest the use of advanced kilns (Friedman, 2000; Greenberg & Porat, 1996; Prub, 2000). The ability of metallic ware potters to control the firing process, the intentional addition of flux to the paste and the surface vitrification represent significant improvements on earlier ceramic pyrotechnology (Friedman, 2000; Greenberg & Porat, 1996; Mellink, 1993).

The KBMW seem to share many of these traits: their mineral-tempered hard fabrics and highly decorated surfaces strikingly contrast with the generally low-fired, chaff-tempered, surface-polished and undecorated local contemporary wares (Hacar & Bulu, 2021; Mellaart, 1963; Tuna et al., 2022). Several technical features (including the use of moulds, very regular wall thickness, repetitive manufacturing and decorative techniques, the presence of potter marks) set this group further apart from the panorama of other contemporary productions and suggest a high degree of standardization (Hacar & Yener, 2020). This hypothesis is corroborated by the KBMW's restricted typological range and extremely homogeneous fabric composition found throughout its entire distribution area, which points to a limited number of manufacturing centres (Tuna et al., 2022) (cf. also supplemental material 1).

Published petrographic analysis on six KBMW samples from three sites in the Konya Plain (in the western portion of the study area; see Fig. S1 in supplemental material 2) indicates a non-porous to slightly porous fabric with a low-calcareous matrix and exclusive use of mineral temper, mostly intentionally added serpentinite and quartz (Gait et al., 2018). Wavelength-dispersive X-ray fluorescence (WD-XRF) analysis on the same dataset also shows an internally coherent group very distinct from other contemporary wares because of very high concentrations of Mg, Cr and Ni, along with elevated concentrations of Co and reduced Sr contents (Gait et al., 2018). Instrumental neutron activation (INAA), X-ray diffraction (XRD) and energy-dispersive X-ray (EDX) analyses of six KBMW sherds from Göltepe (37°48′48.47″N/34°56′11.13″E—the closest village is Celaller, ± 1 km; source: Google Earth) (in the eastern portion of the study area; see Fig. S1 in supplemental material 2) also indicate similar patterns, with high concentrations of Mg, Cr, Ni and Co that set them apart from other ceramics at the site and the presence of serpentinite in their fabric (Friedman, 2000). Petrographic and XRD analyses of two KBMW sherds from Tarsus-Gözlükule (36°54′44.62″N/34°53′44.31″E, ± 10 m; source: Google Earth, to the south-east of the main distribution area; see Fig. S1 in supplemental material 2) further reach similar conclusions regarding their chemical composition (Ünlü, 2009).

An aspect that has attracted no analytical attention so far is the existence of two subgroups that have the same fabric composition but are characterized by different surface and fabric colours, what we termed the 'light surface KBMW' (representing about 80% of the total assemblage) and the 'dark surface KBMW' (about 20%) (Tuna et al., 2022). Based on autoptic observations, our archaeological team have previously suggested that these two groups might be related to different firing temperatures (Tuna et al., 2022), since dark surface specimens often display a vitrified surface (see Fig. S2 in supplemental material 2) (cf. also Ünlü, 2009).

Scope

The characteristics of an ancient ceramic vessel depend on various pyrotechnological aspects (including firing temperature, duration of firing, firing atmosphere) as well as raw material composition and post-depositional (taphonomic) factors. Different firing temperatures alter the composition of the clay and any additional mineral inclusions used in pottery manufacture. For example, magnetite is formed only in reducing firing conditions (Dhanapandian et al., 2012; Ravisankar et al., 2010), while CaMg silicates are formed only above 800–900°C (Shoval & Paz, 2015). Thus, determining the conditions of the firing process in ceramic production (including temperature, duration and firing atmosphere) plays a fundamental role in understanding the compositional transformations of clay minerals in ceramics.

In early studies, basic characteristics such as colour, porosity and density have been used to determine the ceramics' firing conditions. However, this approach is applicable only for ceramics fired below 700°C because of several factors including manufacturing techniques and clay types (Rice, 2015). Moreover, this method is not appropriate to determine variables such as burial time or atmospheric conditions (Daszkiewicz et al., 2012; Rice, 2015). Today, petrography and spectroscopy are proven to be an effective approach to the study of the mineral phases in ancient ceramics (Akyuz et al., 2019; Kiruba & Ganesan, 2015; Măruţoiu et al., 2018; Rodríguez et al., 2015; Tanasi et al., 2019). Fourier-transform infrared spectroscopy (FTIR) and XRD are well-established instrumental methods for such analyses, and well-characterized clay types, firing temperatures and atmosphere (Bahçeli et al., 2016; De Benedetto et al., 2002; Papakosta et al., 2020; Polymeris et al., 2014; Sanjurjo-Sánchez, Montero Fenollós, Barrientos & Polymeris, 2018; Sanjurjo-Sánchez, Montero Fenollós & Polymeris, 2018; Velraj et al., 2015). Especially for bulk characterization, FTIR spectroscopy is considered a useful technique because it is inexpensive, non-destructive, easy to use, requires no sample preparation and allows for microsampling, particularly when combined with an attenuated total reflectance

(ATR) probe. It also differs from other spectroscopic techniques with its ability to detect pseudo-amorphous and short-range-ordered thermal phases, such as meta-smectite and meta-kaolinite (Shoval, 2016; Shoval et al., 2011). In this analytical context, XRD has been often used for the verification of the spectral data obtained from FTIR (Akyuz et al., 2007, 2019; Bahçeli et al., 2016; De Benedetto et al., 2002; Kiruba & Ganesan, 2015; Shoval et al., 2011).

Previously published archaeometric studies on KBMW have been conducted on a very limited dataset and have been focused on understanding the mineralogical composition of ceramic samples through XRD, XRF, EDX and petrographic analysis. The first main objective of this study is to provide a comprehensive archaeometric assessment of the KBMW, complementing published results with FTIR analysis of 49 KBMW sherds collected at eight different EBA sites in the Konya Plain (see Fig. S1 in supplemental material 2). We achieve this goal by using FTIR spectroscopy in tandem with chemometrics, employing variables related to mineralogical structure and manufacturing techniques to develop a principal component analysis (PCA) model. The second main objective is to determine the firing conditions of the ceramic samples by evaluating the changes in the mineral phase data obtained from a combination of the second-derivative FTIR spectra and XRD. In order to achieve these goals, the 49 KBMW samples were compared with 10 sherds from contemporary local wares retrieved from sites in the same area.

MATERIAL AND METHODS

Sherd sampling

The analytical dataset consists of 49 sherds of KBMW from eight different sites across the study area (cf. Fig. S1 in supplemental material 2 for their location), as well as 10 sherds of local wares that are also attributable to the same chronological period, *c*.2750–2200 BCE (see supplemental material 3). All samples were collected within the framework of the Konya Regional Archaeological Survey Project (KRASP; www.krasp.net), an archaeological survey focused on the modern administrative districts of Çumra and Karatay in the Konya Plain, Turkey (Massa et al., 2019, 2020, 2021).

The selection process followed three main criteria: (1) to sample as many different locations as possible across the KRASP study area; (2) to investigate also a representative dataset of the dark surface group, so far not analysed in other studies; and (3) to study a limited group of contemporary non-KBMW sherds representative of the local ceramic repertoire for comparative purposes. For this analysis, three main ceramic groupings were therefore identified within the dataset: light surface KBMW, dark surface KBMW and non-KBMW. The samples were cleaned mechanically and impurities were removed with ultra-pure water. Approximately 2 g of sample were selected and ground using a hand-held agate mortar. All selected samples were subjected to FTIR analysis, and a subset of eight sherds was further selected for XRD analysis (see supplemental material 6) as representative specimens of the major ceramic groups identified through the FTIR-related chemometric modelling. A representative sample of shapes and surfaces of the analysed sherds are given in Fig. S3 in supplemental material 2.

FTIR analysis

The functional groups giving information about the mineral phases of the samples were analysed with a Bruker Tensor II FTIR spectrometer (Bruker Optic GmbH, Ettlingen, Germany) equipped with a single-bounce diamond ATR, a crystal deuterated triglycine sulfate detector. The spectral data were obtained covering the 4000–400 cm^{-1} range with a scan

number of 128 and resolution number of 4 cm^{-1}. The 50 mg sample was uniformly spread on the ATR surface, and a new background was recorded between each scan.

XRD analysis

The XRD analysis was employed to determine the major crystalline phases of samples selected as a result of the chemometric analysis. The analysis was carried out using a Bruker D8 Advance XRD powder diffractometer (Bruker Optic). The patterns were recorded with CuKα radiation (wavelength $\lambda = 1.5406$ Å, 40 mA, 45 kV) at 0.020 steps at the rate of 0.5/s over range $5 < 2\theta < 110$. The results provide estimates on quantitative percentages based on external standard methods.

Chemometric modelling

Chemometric processing and modelling were performed using the Omnic software (Thermo Fisher Scientific, USA) and the Unscrambler software (CAMO, ASA, Norway). In total, 59 sherd samples were scanned with FTIR to characterize mineralogical differences in the samples, and the spectral information obtained from FTIR was used to create six different PCA models. In the PCA models, second-derivative FTIR spectra were used in the range 1500–400 cm^{-1}. The smoothing process of the Savitzky–Golay method (Savitzky & Golay, 1964) was tested with an array of different numbers of smoothing points (3, 9, 17, 25, 33 and 41) to reveal the effects on the statistical performance of the models and to determine whether they have effects in reducing the errors. The statistical performances of the models developed were evaluated by the number of samples outside of the explained variance (95%) and the eigen value. To identify the best PCA model, while the number of samples outside of the explained variance was considered as small as, the eigen value was considered as big as possible. The results of the best PCA model were also subjected to hierarchical cluster analysis (HCA, Euclidian distance) to reflect the different sherd groups with a linear distribution. The main sample groups were determined according to the best PCA model. In order to better identify the mineral phases and to obtain semi-quantitative results from the FTIR data, the peak deconvolution process was applied to the about 1200–750 cm^{-1} range of the raw average spectrum of each ceramic group by using Origin software (OriginLab, MA, USA). This ensured that the overlapped peaks are visible. During the peak deconvolution process, the fit was converged until reaching the Chi^2 tolerance of 1.10^{-9}. For the XRD analysis, samples representing each main group were selected, and a separate PCA model was created for the quantitative data to be further compared with the FTIR data.

RESULTS

Discrimination of the ceramic samples using chemometric modelling

FTIR spectra of the 59 sherds in the range of 4000–400 cm^{-1} are given in Figure 2 (f). The spectra show that the samples are contained by OH bendings of H_2O (3500–3200 and 1641 cm^{-1}) (Dhanapandian et al., 2012; Kiruba & Ganesan, 2015; Măruţoiu et al., 2018; Velraj et al., 2015), OH bendings of meta-smectite (1634 cm^{-1}) (Shoval & Paz, 2015), and bendings out-of-plane mode of calcite (1431, 1417 cm^{-1}) (Akyuz et al., 2019; Kiruba & Ganesan, 2015; Măruţoiu et al., 2018; Papakosta et al., 2020; Ravisankar et al., 2010; Sanjurjo-Sánchez Montero Fenollós, Barrientos & Polymeris, 2018; Shoval, 2003; Shoval et al., 2011; Shoval &

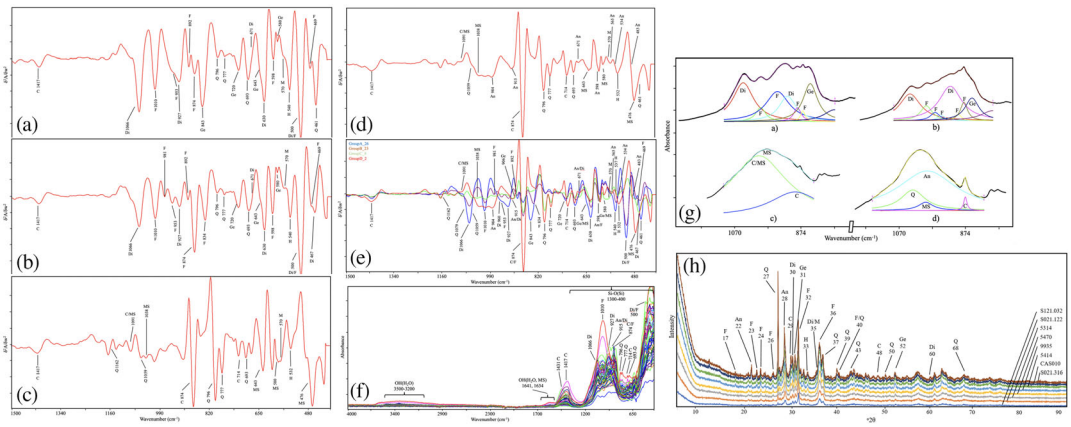

FIGURE 2 Analytical spectra of the ceramic samples: (a–d) statistically average second-derivative Fourier-transform infrared spectrometer (FTIR) spectra with 17 smoothing points of all sherd groups in the range of 1500–400 cm^{-1}; (e) overlaid spectra for all groups; (f) FTIR spectra of 59 ceramic samples in the range of 4000–400 cm^{-1}; (g) vibration bands of overlapped mineral phases in the raw spectra; and (h) X-ray diffraction (XRD)-powder diffraction patterns of selected sherds. An, anorthite; C, calcite; Di, diopside; F, forsterite; Ge, gehlenite; H, hematite; M, magnetite; MS, meta-smectite; and Q, quartz. Details of all spectra given together can be accessed in supplementary material 4

Paz, 2015). Also, asymmetric stretching, bending and intensive rocking of Si-O (Si) bonds of the different mineral phases are seen in the range of 1300–400 cm^{-1} (Lucovsky et al., 1987; Sanjurjo-Sánchez, Montero Fenollós & Polymeris, 2018; Yu et al., 2003). Strong absorbances of CaMg silicates, such as diopside and forsterite, stand out at 1066, 927, 915 and 500 cm^{-1} (De Benedetto et al., 2002; Rruff, 2021c) and 1010, 874 and 500 cm^{-1} (Rruff, 2021d; Tarte, 1963), respectively. The mineral phases anorthite (915 cm^{-1}) (Rruff, 2021a), calcite (874 and 714 cm^{-1}) (Barilaro et al., 2008; De Benedetto et al., 2002; Măruţoiu et al., 2018; Papakosta et al., 2020; Rruff, 2021b; Sanjurjo-Sánchez, Montero Fenollós, Barrientos & Polymeris, 2018; Shoval, 2003), and quartz (796, 777 and 693 cm^{-1}) (Akyuz et al., 2007, 2008, 2019; Barilaro et al., 2008; De Benedetto et al., 2002; Dhanapandian et al., 2012; Kiruba & Ganesan, 2015; Papakosta et al., 2020; Sanjurjo-Sánchez, Montero Fenollós, Barrientos & Polymeris, 2018; Shoval, 2003; Shoval & Paz, 2015; Velraj et al., 2015) were also observed.

A second-derivative analysis was employed on FTIR data in order to identify underlying peaks and assign the mineralogical composition of the samples. This process is a highly efficient method for the identification of peaks that are otherwise not clearly detectable on the raw FTIR spectra, as it enhances the resolution (Ami et al., 2013), and is widely applied in the mineralogical investigations of ceramic samples (Akyuz et al., 2019; De Benedetto et al., 2002; Shoval et al., 2011; Shoval & Paz, 2015; Tarhan et al., 2021).

Because ATR-FTIR spectra can have a low signal/noise ratio, the second-derivative process has the potential to increase spectral noise, and therefore smoothing is one of the most common approaches to managing unwanted noise contributions (Nunes, 2014). If a simple smoothing procedure were carried out for one spectrum at a time along the wavenumber axis, we would expect a loss in data. Thus, in order to minimize both data loss and smoothing, special noise reduction methods use the multivariate nature of the spectral dataset. Savitzky–Golay smoothing filters employing smoothing points are frequently used for this purpose and they are often used to render visible the relative widths and heights of spectral lines in noisy spectrometric data (Press & Teukolsky, 1990). For this study, different numbers of smoothing points (3, 9, 17, 25, 33 and 41) were applied to FTIR results in the range of 1500–400 cm^{-1} and six different PCA models were developed (see supplemental material 4).

The statistical performance of the PCA models was first evaluated through the number of samples outside the explained variance (95%) and the models' eigen value (see supplemental material 4). The PCA model with three smoothing points has the lowest number of samples outside of the explained variance and also the lowest eigen value. These explained variances define outliers that decrease the statistical success of the developed PCA models. Since this study's goal was to determine the large-scale tendencies of 59 sherd samples, the outlier number with an efficient eigen value was aimed to be minimum or zero if possible. It was observed that the eigen values of the PCA models developed with the smoothing point values above 17 slightly increased, but the number of outliers also increased due to high data loss. For this reason, the PCA model with 17 smoothing points (PCA model 3) was chosen as the most successful PCA model for this study. Statistical plots of the PCA models are given in supplemental material 4.

The influence plot obtained from the best PCA model is given in Figure 3 (a). This plot allows to understand whether all data fall within the model space using 5% as the significance level for the critical distance. The *y*-axis shows the *F*-residuals, which represent the amount of information remaining after estimating the data. Hotelling's T^2 (*x*-axis in Fig. 3a) indicates the distance from the centre of the best PCA model. For a robust model, all the analysed samples

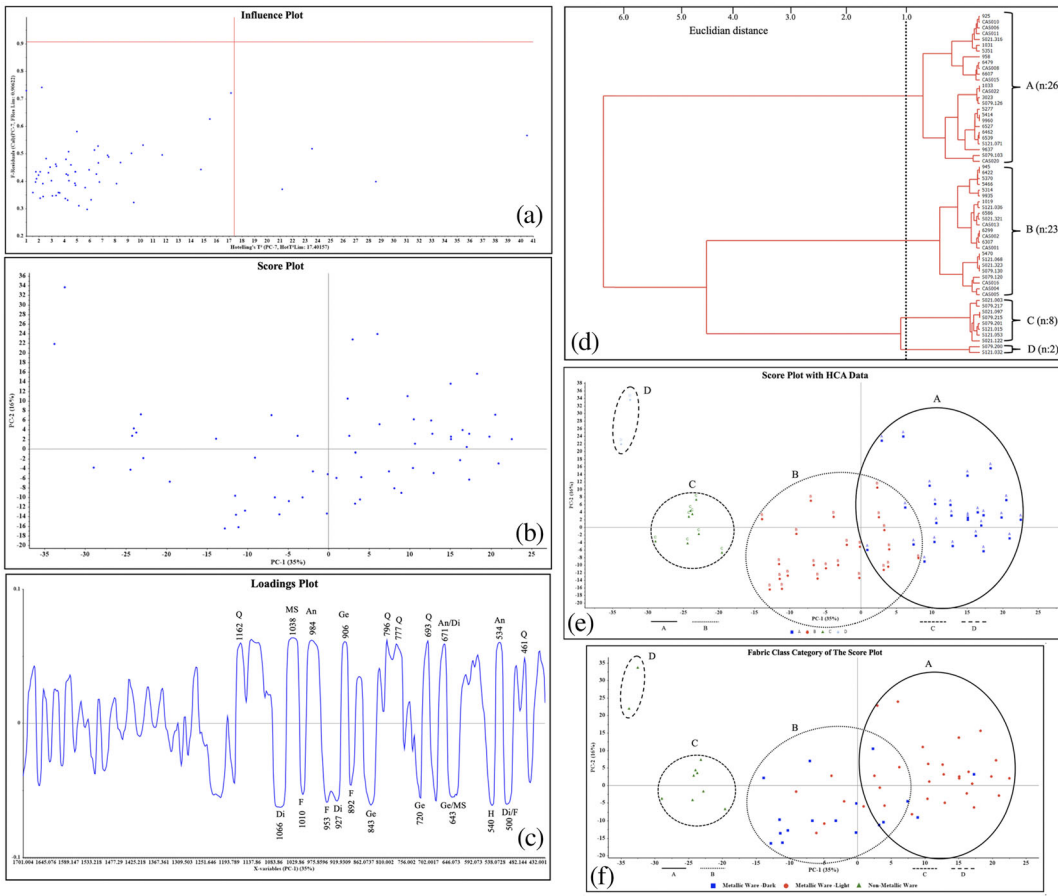

FIGURE 3 Statistical plots of the best principal component analysis (PCA) model obtained from Fourier-transform infrared spectrometer (FTIR) analysis: (a) influence; (b) score; (c) loadings; (d) dendrogram; (e) score plot categorized by hierarchical cluster analysis (HCA); and (f) score plot categorized by fabric class. An, anorthite; Di, diopside; F, forsterite; Ge, gehlenite; H, hematite; MS, meta-smectite; and Q, quartz

should be within the area indicated by the horizontal and vertical red lines in Figure 3 (a). As the number of samples located outside the specified area increases, the proposed PCA model moves away from the centre and the classification performance of the model decreases. Figure 3 (a) shows that most of the samples are located within the area and the classification capability of the developed model is sufficient.

Figure 3 (b) shows the score plot, which is a graphical representation of the distribution and configuration of the samples in the best PCA model. The score plot indicates that PC1 explains 35% of the variance, while PC2 explains 16%; therefore, 51% of the variance is described by the first two PCs. All sherd samples were mostly contributing to PC1 (35%) and were classified based on the differences represented by PC1.

Figure 3 (c) shows the loadings plot obtained from the best PCA model. This plot highlights the most effective mineral phases that played a role in the formation of the best PCA model. The loadings plot in Figure 3 (c) reveals that the mineral phases of quartz, diopside, meta-smectite, forsterite, anorthite, gehlenite and hematite are the most important mineralogical structures that contribute at least 0.1% in the positive or negative direction for the formation of PC1 and PC2.

A dendrogram plot was created using second-derivative spectra with 17 smoothing points to determine a one-dimensional cluster formation of the samples classified with the best PCA model, employing differences in the mineralogical structure. Figure 3 (d) presents the dendrogram plot developed for the samples using HCA with the Euclidian method. Based on their mineralogical structure, the ceramic sherds were separated into four main groups (A–D) by the best PCA model at a Euclidian distance of 1.0 units. The score plot of the best PCA model was drawn according to the HCA distribution and is given in Figure 3 (e).

Figure 3 (f) shows the score plot compared with the three main fabric classes selected for analysis (non-KBMW, light surface KBMW and dark surface KBMW; cf. supplemental material 6). Non-KBMW samples are clearly distinct from KBMW pieces and cluster within groups C and D to the left of the plot. While partly overlapping, there is a strong tendency for light surface KBMW and dark surface KBMW to separate into groups A and B, respectively.

Assessing firing conditions through FTIR results

The statistically average second-derivative FTIR spectra with 17 smoothing points of all sherd groups in the range of 1500–400 cm^{-1} are given in Figure 2 (a–d) for sherd groups A–D, respectively. Their overlaid spectra are shown in Figure 2 (e). The mineral phases of calcite, meta-smectite, quartz, anorthite, gehlenite, diopside, forsterite, magnetite and hematite were diagnosed. In particular, anorthite, gehlenite, diopside, magnetite, hematite and meta-smectite were used to determine the firing conditions of the analysed ceramics. The forsterite mineral detected in the infrared spectra was not used in the interpretation of the firing temperatures of the studied samples, since its likely source may have been the serpentinite inclusions that published petrographic analysis shows to have been intentionally added in the KBMW as a flux (Gait et al., 2018).

The FTIR bands of the mineral structures detected in the samples are given in supplemental material 4 together with related references. Firing temperatures up to 800°C cause dihydroxylation of calcite (Maggetti et al., 2011; Shoval et al., 1993) to form CaO (Fabbri et al., 2014; Shoval et al., 1993). Calcite mineral, commonly detected in ancient ceramics, is often a result of re-carbonization of degraded calcite especially if coexisting with highly fired minerals such as diopside and gehlenite. For this reason, the presence of calcite mineral was not employed to assess the firing conditions of the dataset.

The anorthite phase is stable up to about 1050°C. CaMg silicate contributions were also monitored with the 906, 843, 720, 643 and 580 cm^{-1} peaks corresponding to gehlenite

(De Benedetto et al., 2002; Shoval & Paz, 2015), 1066, 960, 927, 915, 671, 630, 500 and 467 cm^{-1} attributable to diopside (De Benedetto et al., 2002; Rruff, 2021c), and 1010, 981, 953, 892, 874, 834, 598, 500 and 469 cm^{-1} pertaining to forsterite (Choudhary et al., 2017; Rruff, 2021d; Tarte, 1963). Only firing temperatures above 800°C allow the formation of these high-temperature minerals. This result indicates that calcite minerals with CaMg silicates were formed in the re-carbonization process or post-burial decomposition (Ravisankar et al., 2010).

In addition, the presence of magnetite and hematite sheds light on the nature of the firing atmosphere: magnetite indicates reducing atmosphere and results in grey-black ceramic surfaces, while hematite points to an oxidizing atmosphere and creates a red-hued surface.

The plots of average raw spectra of the ceramic groups in the range of 1200–750 cm^{-1} where peak deconvolution process can be applied are given in Figure 2 (g). Vibration bands of overlapping diopside, forsterite, gehlenite, calcite, meta-smectite and anorthite mineral phases in the raw spectrum of the relevant range can be observed thanks to the peak deconvolution process. This process allows the easy determination of the semi-quantitative ratios of ceramic groups containing these minerals, using FTIR data.

The semi-quantitative results of the FTIR analysis (summarized in Table 1) make clear that samples from groups C and D have been fired at about 600–800°C due to the absence of CaMg silicates and the relative abundance of meta-smectite. In particular, ceramics belonging to group D contain a high amount of calcite and anorthite. Conversely, the relatively high proportions of diopside mineral in groups A and B indicate firing temperatures reaching up to and above 800°C. The relative abundance of Fe oxides also shows that groups A, B and D have mostly been produced in an oxidizing firing atmosphere, while group C has mostly been produced in a relatively reducing environment. Due to the presence of calcite and meta-smectite, it can also be concluded that the analysed samples have been produced from a calcareous clay with smectitic character.

XRD results

Semi-quantitative analysis was carried out along with the diffraction pattern analysis for calcite, quartz, diopside, gehlenite, forsterite, anorthite, hematite and magnetite. The references of the determined mineral phases in the sherd samples and the relative abundance of these minerals by XRD are given in supplemental material 4 and Table 2, respectively.

XRD patterns of samples from groups C and D were dominated by the quartz signal (Figure 2, h), confirming the FTIR results. In particular, sample S121.032 (group D) contains more calcite mineral than all other samples. The highest ratios of calcite, quartz and magnetite are found in samples S021.122 (group C) and S121.032 (group D). In addition, forsterite is absent in samples from groups C and D. Sherds belonging to groups A (S021.316, CAS010, 5414) and B (99-35, 5470, 5314) stand out with their high forsterite, diopside and gehlenite ratios, and the highest forsterite ratios are found in group A (Table 2).

TABLE 1 Semi-quantitative distribution of the mineralogical phases in the analysed sherds according to Fourier-transform infrared spectrometer (FTIR) analysis

Sherd group	*C*	*Q*	*Di*	*Ge*	*F*	*An*	*M*	*H*	*MS*
A	*	*	***	*	****	–	Tr	****	–
B	*	*	****	*	**	–	Tr	**	–
C	***	***	–	–	–	–	**	*	**
D	****	****	–	–	–	**	Tr	**	*

C, calcite; Q, quartz; An, anorthite; Ge, gehlenite; Di, diopside; F, forsterite, M, magnetite; H, hematite; and MS, meta-smectite. The number of asterisks indicates the abundance of the mineralogical abundance. tr, Trace amount.

TABLE 2 Semi-quantitative mineralogical composition of the analysed samples according to X-ray diffraction (XRD) analysis

Sherd group	*Sample number*	*C*	*Q*	*Di*	*Ge*	*F*	*An*	*H*	*M*
A	S021.316	*	*	***	**	**	–	**	Tr
A	CAS010	*	*	***	**	**	–	**	Tr
A	5414	*	*	****	*	**	–	**	Tr
B	99-35	*	**	***	**	*	–	**	Tr
B	5470	*	**	***	*	*	–	**	Tr
B	5314	*	**	***	**	*	–	**	Tr
C	S021.122	***	****	–	–	–	–	Tr	*
D	S121.032	****	****	–	–	–	**	**	*

C, calcite; Di, diopside; F, forsterite, An, anorthite; Ge, gehlenite; H, hematite; M, magnetite; and Q, quartz. The number of asterisks indicates the abundance of the mineralogical abundance. tr: Trace amount.

The FTIR and XRD analyses conducted in this study indicate an abundance of Mg oxides in all KBMW samples, including prominently diopside and forsterite, and this confirms earlier research on the same class of materials from the broader region (Friedman, 2000; Gait et al., 2018; Ünlü, 2009). The results also strongly suggest that this ceramic production was produced at temperatures of 800°C and possibly above. This is not only significantly higher than other contemporary ceramic products in this study (between about 600 and 800°C), but also higher than firing temperatures of other contemporary pottery assemblages in western Anatolia (not exceeding 800°C; Semiz et al., 2018). Preliminary analysis on polished sections of samples from the KBMW light and dark surface subgroups indicate clear differences in the firing conditions (see Fig. S2 in supplemental material 2). While displaying the same inclusions in similar proportions, dark surface specimens often show vitrified surfaces, a process that is never visible in light surface examples. Even if we are currently not able to narrowly bracket a temperature range for the two KBMW subgroups, we can with some confidence suggest that the dark surface products would have been exposed to overall higher firing conditions. Dark surface sherds are present at numerous sites across the Konya Basin and represent 20% of all sherds (Tuna et al., 2022), suggesting that these were intentional products rather than manufacturing (overfired) discards.

Our results further show that KBMW were produced in oxidizing firing atmospheres, while other analysed local wares were fired in reducing environments.

DISCUSSION

Numerous characteristics set the KBMW apart from other local wares, including differences in clay preparation, production techniques and pyrotechnology (Friedman, 2000; Gait et al., 2018; Hacar, 2017; Hacar & Bulu, 2021). From a morpho-typological perspective, only 45% of KBMW types are paralleled in local contemporary wares, and the KBMW form repertoire is overall rather limited when compared with other ceramic groups (Tuna et al., 2022). Previously published chemical composition analyses on EBA ceramics across the study area further throw in high relief the homogeneity of chemical signatures within the KBMW group and—in contrast—the uniqueness of these signatures against the panorama of southern-central Anatolian ceramics (Friedman, 2000; Gait et al., 2018; Ünlü, 2009). These disparate strands of evidence point to the KBMW being manufactured with recipes and techniques than were shared among all KBMW potters but at the same time were very different from other contemporary ceramic productions.

This study also indicates that KBMW vessels were fired at higher temperatures than other contemporary wares in the region, a pattern that suggests the use of advanced ceramic kilns. This hypothesis is corroborated by the overall rarity of mottled surfaces and/or visible cores in KBMW products, indicative of good control of the firing conditions. Another evidence pointing in this direction is the consistent presence of potter marks on handles. This pattern starkly contrasts with the absence of similar signs in other pottery groups and is suggestive of multiple potters using the same kiln (Hacar & Yener, 2020).

Lastly, in our fieldwork project (KRASP) we encountered much higher ratios of KBMW at major centres (e.g., Karhane Höyük, Samıh Höyük, Sarlak Höyük and Seyithan Höyük), a pattern also observed by others in the same area (Baird, 1998) and in the Karaman Plain further south (Kamış, 2019). This suggests either a preferential access to KBMW by certain communities and/or the localization of its manufacture restricted to a small number of centres.

Taken together, these elements support the hypothesis of the existence of both specialized workshops focusing on KBMW products, and of professional potters who shared a similar technological knowledge, already by the early third millennium BCE. The absence of excavated manufacturing contexts does not allow to delve further into the degree of socio-economic complexity of KBMW workshops. However, they occur in a pivotal phase for central Anatolian history, when a marked increase in socio-political complexity of the local communities becomes visible across numerous proxies including monumental buildings, elite-sponsored feasting, elite graves and elite-specific burial customs (Bachhuber, 2011, 2015; Düring, 2011; Massa, 2014). At the same time, craft specialization becomes common in a number of economic activities such as metallurgy (Lehner & Yener, 2014; Yener, 2000), textile industry, luxury goods manufacture (Bachhuber, 2015; Fidan et al., 2015), and trade (Massa & Palmisano, 2018). From the mid-third millennium BCE, the production of large (up to 2.5 m high) pithoi (e.g., at Kumyer; Büyüközer et al., 2019) and the diffusion of the potter's wheel (Kamış, 2018; Türkteki, 2014) both provide evidence for increased specialization in pottery production as well. In this light, the integration of the results of this study with previously published archaeometric and morpho-typological analyses indicates that KBMW can be considered the first documented specialized ceramic production in central Anatolia.

CONCLUSIONS

In this study, FTIR and XRD analyses were to assess the firing conditions of KBMW samples from different EBA (2700–2200 BCE) sites in central Anatolia. The analytical results show that FTIR analysis is effective in characterizing and classifying different ceramic groups, analysing large numbers of samples with low cost and fast analytical time, as well as in detecting pseudo-amorphous and short-range-ordered thermal phases that cannot be detected by XRD analysis. The methods developed here can be easily applied to other case studies.

ACKNOWLEDGEMENTS

The authors thank Ömer Faruk Türkan, director of the Konya Museum of Archaeology, for providing the permit to study the samples employed in this research. The authors are also grateful to the Scientific Research Projects Foundation of Selçuk University for the financial support of this work.

COMPLIANCE WITH ETHICAL STANDARDS

The authors report no conflict of interest.
The authors report that this research involving no human participants and/or animals.
The authors report that there is no informed consent.

CREDIT AUTHOR STATEMENT

İsmail Tarhan: conceptualization, methodology, software, data curation, writing—original draft preparation, visualization, investigation, supervision, validation, resources, writing, reviewing and editing, funding acquisition. **Michele Massa**: project administration, conceptualization, methodology, funding acquisition, resources, investigation, writing—original draft preparation, writing—reviewing and editing. **Yusuf Tuna**: conceptualization, resources, investigation. **Fatma Şahin**: investigation.

PEER REVIEW

The peer review history for this article is available at https://publons.com/publon/10.1111/arcm.12812.

DATA AVAILABILITY STATEMENT

The data that support the findings of this study are available in the supplementary material of this article.

ORCID

İsmail Tarhan https://orcid.org/0000-0003-3353-8635

REFERENCES

Akyuz, S., Akyuz, T., Basaran, S., Bolcal, C., & Gulec, A. (2007). FT-IR and micro-Raman spectroscopic study of decorated potteries from VI and VII century BC, excavated in ancient Ainos—Turkey. *Journal of Molecular Structure*, *834–836*, 150–153. https://doi.org/10.1016/j.molstruc.2006.12.011

Akyuz, S., Akyuz, T., Basaran, S., Bolcal, C., & Gulec, A. (2008). Analysis of ancient potteries using FT-IR, micro-Raman and EDXRF spectrometry. *Vibrational Spectroscopy*, *48*(2), 276–280. https://doi.org/10.1016/j.vibspec.2008.02.011

Akyuz, S., Guliyev, F., Celik, S., Ozel, A. E., & Alakbarov, V. (2019). Investigations of the Neolithic potteries of 6th millennium BC from Göytepe-Azerbaijan by vibrational spectroscopy and chemometric techniques. *Vibrational Spectroscopy*, *105*, 102980. https://doi.org/10.1016/j.vibspec.2019.102980

Ami, D., Mereghetti, P., & Maria, S. (2013). Multivariate analysis for Fourier transform infrared spectra of complex biological systems and processes. In L. Freitas (Ed.), *Multivariate analysis in management, engineering and the sciences*. In Tech Open. https://doi.org/10.5772/53850

Bachhuber, C. (2011). Negotiating metal and the metal form in the royal tombs of Alacahöyük in north-central Anatolia. In T. C. Wilkinson, S. Sherratt, & J. Bennet (Eds.), *Interweaving worlds: Systemic interactions in Eurasia, 7th to 1st millennia BC: Memorial volume for Professor Andrew Sherratt* (pp. 158–174). Oxbow Books. https://doi.org/10.2307/j.ctvh1dr2k.17

Bachhuber, C. (2015). *Citadel and cemetery in early bronze age Anatolia*. Equinox.

Bahçeli, S., Güleç, G., Erdoğan, H., & Söğüt, B. (2016). Micro-Raman and FT-IR spectroscopic studies of ceramic shards excavated from ancient Stratonikeia city at Eskihisar village in west–South Turkey. *Journal of Molecular Structure*, *1106*, 316–321. https://doi.org/10.1016/j.molstruc.2015.10.036

Baird, D. (1998). Konya Plain. *Anatolian Archaeology*, *4*, 16.

Barilaro, D., Barone, G., Crupi, V., Majolino, D., Mazzoleni, P., Tigano, G., & Venuti, V. (2008). FT-IR absorbance spectroscopy to study Sicilian 'proto-majolica' pottery. *Vibrational Spectroscopy*, *48*(2), 269–275. https://doi.org/10.1016/j.vibspec.2008.01.005

Büyüközer, A., Gider-Büyüközer, Z., & Tırpan, A. A. (2019). Börükçü Kazılarında Açığa Çıkarılan Seramik Fırınları: Kumyer, Börükçü ve Beybağ Örnekleri. In Ö. Dumankaya (Ed.), *Çağlar Boyunca Üretim ve Ticaret: Prehistorya'dan Bizans Dönemi'ne* (pp. 387–412). Bilgin Kültür Sanat Yayınları.

Choudhary, R., Manohar, P., Vecstaudza, J., Yáñez-Gascón, M. J., Sánchez, H. P., Nachimuthu, R., Locs, J., & Swamiappan, S. (2017). Preparation of nanocrystalline forsterite by combustion of different fuels and their comparative in-vitro bioactivity, dissolution behaviour and antibacterial studies. *Materials Science and Engineering: C*, *77*, 811–822. https://doi.org/10.1016/j.msec.2017.03.308

Daszkiewicz, M., van Ess, M., & Schneider, G. (2012). Pottery and clay from Uruk, southern Iraq. Laboratory analysis of pottery fabrics from the late Uruk to the Seleucid period. *Zeitschrift für Orient-Archäologie*, *5*, 90–102.

De Benedetto, G. E., Laviano, R., Sabbatini, L., & Zambonin, P. G. (2002). Infrared spectroscopy in the mineralogical characterization of ancient pottery. *Journal of Cultural Heritage*, *3*(3), 177–186. https://doi.org/10.1016/S1296-2074(02)01178-0

Dhanapandian, S., Manoharan, C., & Sutharsan, P. (2012). Applications of FTIR and 57 Fe Mössbauer techniques in studies of recently excavated Indian archaeological pottery. *Acta Physica Polonica a*, *121*, 592–598. https://doi.org/10.12693/APhysPolA.121.592

Düring, B. (2011). *The prehistory of Asia minor: From complex hunter–gatherers to early urban societies: Cambridge*. Cambridge University Press.

Fabbri, B., Gualtieri, S., & Shoval, S. (2014). The presence of calcite in archeological ceramics. *Journal of the European Ceramic Society*, *34*(7), 1899–1911. https://doi.org/10.1016/j.jeurceramsoc.2014.01.007

Fidan, E., Sarı, D., & Türkteki, M. (2015). An overview of the Western Anatolian early bronze age. *European Journal of Archaeology*, *18*(1), 60–89. https://doi.org/10.1179/1461957114Y.0000000070

Friedman, E. S. (2000). Technological Style in Early Bronze Age Anatolia: The Interrelationship Between Ceramic And Metal Production At Göltepe, the University of Chicago, Chicago, Illinois.

Gait, J., Müller, N. S., Kiriatzi, E., & Baird, D. (2018). Examining the Dynamics of Early Bronze Age Pottery Production and Distribution in the Konya Plain of South Central Anatolia, Turkey. In E. Alram-Stern & B. Horejs (Eds.), *Pottery technologies and sociocultural connections between the Aegean and Anatolia during the 3rd millennium BC*. Österreichische Akademie der Wissenschaften, Philosophisch-historische Klasse. https://doi.org/10.2307/j.ctv8xnj5p.8

Greenberg, R., & Porat, N. (1996). A third millennium Levantine pottery production center: Typology, petrography, and provenance of the metallic ware of northern Israel and adjacent regions. *Bulletin of the American Schools of Oriental Research*, *301*, 5–24. https://doi.org/10.2307/1357293

Hacar, A. (2017). İlk Tunç Çağı'na Tarihlenen Anadolu Metalik Çanak Çömleğine İlişkin Yeni Bilgiler: Göltepe Buluntuları. *Adalya*, *20*, 21–40.

Hacar, A., & Bulu, M. (2021). Early Bronze Age Pottery Wares. In A. K. Yener (Ed.), *Göltepe excavations. Tin production at an early bronze age mining town in the central Taurus Mountains, Turkey* (pp. 77–81). INSTAP Academic Press.

Hacar, A., & Yener, A. (2020). Anatolian pot Marks in the 3rd millennium BC: Signage, early state formation, and organization of production. *Adalya*, *23*, 25–58.

Kamış, Y. (2018). Acemhöyük Buluntuları Işığında Erken Tunç Çağı'nda Orta Anadolu'nun Güneyinde Çark Yapımı Seramiğin Ortaya Çıkışı. *Adalya*, *21*, 63–84.

Kamış, Y. (2019). Karaman Eminler Höyük Archaeological Survey Project: Preliminary Results of the 2016–2018 Seasons. In S. Steadman & G. McMahon (Eds.), *The archaeology of Anatolia, volume III: Recent discoveries (2017–2018)* (pp. 231–245). Cambridge Scholars.

Kiruba, S., & Ganesan, S. (2015). FT-IR and micro-Raman spectroscopic studies of archaeological potteries recently excavated in Poompuhar, Tamilnadu, India. *Spectrochimica Acta Part a: Molecular and Biomolecular Spectroscopy*, *145*, 594–597. https://doi.org/10.1016/j.saa.2015.03.055

Lehner, J. W., & Yener, A. K. (2014). Organization and Specialization of Early Mining and Metal Technologies in Anatolia. In B. W. Roberts & C. P. Thornton (Eds.), *Archaeometallurgy in global perspective* (pp. 529–557). Springer. https://doi.org/10.1007/978-1-4614-9017-3_20

Lucovsky, G., Mantini, M. J., Srivastava, J. K., & Irene, E. A. (1987). Low-temperature growth of silicon dioxide films: A study of chemical bonding by ellipsometry and infrared spectroscopy. *Journal of Vacuum Science & Technology, B: Microelectronics Processing and Phenomena*, *5*(2), 530–537. https://doi.org/10.1116/1.583944

Maggetti, M., Neururer, C., & Ramseyer, D. (2011). Temperature evolution inside a pot during experimental surface (bonfire) firing. *Applied Clay Science*, *53*(3), 500–508. https://doi.org/10.1016/j.clay.2010.09.013

Măruţoiu, C., Bratu, I., Ţiplic, M. I., Măruţoiu, V. C., Nemeş, O. F., Neamţu, C., & Hernanz, A. (2018). FTIR analysis and 3D restoration of Transylvanian popular pottery from the XVI–XVIII centuries. *Journal of Archaeological Science: Reports*, *19*, 148–154. https://doi.org/10.1016/j.jasrep.2018.02.044

Massa, M. (2014). Early bronze age burial customs on the central Anatolian plateau: A view from Demircihöyük-Sarıket. *Anatolian Studies*, *64*, 73–93. https://doi.org/10.1017/S0066154614000064

Massa, M., Bachhuber, C., Şahin, F., Bostancı-Kolankaya, N., & Tuna, Y. (2019). The Konya regional archaeological survey project: The 2017 and 2018 field seasons. *Anatolica*, *XLV*, 159–180.

Massa, M., Bachhuber, C., Şahin, F., Erpehlivan, H., & Lauricella, A. J. (2021). The 2019 and 2020 seasons of the Konya regional archaeological survey project. *Anatolica*, *XLVII*, 215–242.

Massa, M., Bachhuber, C., Şahin, F., Erpehlivan, H., Lauricella, A. J., & Osborne, J. (2020). A landscape-oriented approach to urbanisation and early state formation in the Konya and Karaman Plains, Turkey. *Anatolian Studies*, *70*, 45–75. https://doi.org/10.1017/S0066154620000034

Massa, M., & Palmisano, A. (2018). Change and continuity in the long-distance exchange networks between western/Central Anatolia, northern Levant and northern Mesopotamia, c. 3200–1600 BCE. *Journal of Anthropological Archaeology*, *49*, 65–87. https://doi.org/10.1016/j.jaa.2017.12.003

Mellaart, J. (1963). Early cultures of the south Anatolian plateau, II: The late chalcolithic and early bronze ages in the Konya plain. *Anatolian Studies*, *13*, 199–236. https://doi.org/10.2307/3642494

Mellink, M. (1993). The Anatolian South Coast in the Early Bronze Age: The Cilician Perspective. In M. Frangipane, H. Hauptmann, M. Liverani, P. Matthiae, & M. Mellink (Eds.), *Between the Rivers and over the mountains: Alba Palmieri Dedicata* (pp. 495–508). University of Rome.

Nunes, C. A. (2014). Vibrational spectroscopy and chemometrics to assess authenticity, adulteration and intrinsic quality parameters of edible oils and fats. *Food Research International*, *60*, 255–261. https://doi.org/10.1016/j.foodres.2013.08.041

Papakosta, V., Lopez-Costas, O., & Isaksson, S. (2020). Multi-method (FTIR, XRD, PXRF) analysis of Ertebølle pottery ceramics from Scania, southern Sweden. *Archaeometry*, *62*, 677–693. https://doi.org/10.1111/arcm.12554

Polymeris, G. S., Kiyak, N. G., Koul, D. K., & Kitis, G. (2014). The firing temperature of pottery from ancient Mesopotamia, Turkey, using luminescence methods: A case study for different grain-size fractions. *Archaeometry*, *56*(5), 805–817. https://doi.org/10.1111/arcm.12044

Press, W. H., & Teukolsky, S. A. (1990). Savitzky-Golay smoothing filters. *Computers in Physics*, *4*(6), 669–672. https://doi.org/10.1063/1.4822961

Prub, A. (2000). The Metallic Ware of Upper Mesopotamia: definition, chronology and distribution. In *Chronologies des pays du Caucase et de l'Euphrate aux IVe–IIIe millénaires. Actes du Colloque d'Istanbul, 16–19 décembre 1998* (pp. 193–203). Institut Français d'Études Anatoliennes.

Ravisankar, R., Kiruba, S., Pachamuthu, E., Senthilkumar, G., & Chandrasekaran, A. (2010). Mineralogical characterization studies of ancient potteries of Tamilnadu, India by FT-IR spectroscopic technique. *E-Journal of Chemistry*, *7*, S185–S190.

Rice, P. M. (2015). *Pottery analysis, second edition: A sourcebook*. The University of Chicago Press. https://doi.org/10.7208/chicago/9780226923222.001.0001

Rodríguez, C., Bermúdez Coronel-Prats, R., Barone, G., Cultrone, G., Mazzoleni, P., & Tanasi, D. (2015). Petrographic and chemical characterization of bronze age pottery from the settlement of mount san Paolillo (Catania, Italy). *Rendiconti Lincei*, *26*(4), 485–497. https://doi.org/10.1007/s12210-015-0421-6

Rruff. (2021a). The integrated database of X-ray diffraction and FT-IR data for anorthite mineral.

Rruff. (2021b). The integrated database of X-ray diffraction and FT-IR data for calcite mineral.

Rruff. (2021c). The integrated database of X-ray diffraction and FT-IR data for diopside mineral.

Rruff. (2021d). The integrated database of X-ray diffraction and FT-IR data for forsterite mineral.

Sanjurjo-Sánchez, J., Montero Fenollós, J. L., Barrientos, V., & Polymeris, G. S. (2018). Assessing the firing temperature of Uruk pottery in the middle Euphrates Valley (Syria): Bevelled rim bowls. *Microchemical Journal*, *142*, 43–53. https://doi.org/10.1016/j.microc.2018.06.009

Sanjurjo-Sánchez, J., Montero Fenollós, J. L., & Polymeris, G. S. (2018). Technological aspects of Mesopotamian Uruk pottery: Estimating firing temperatures using mineralogical methods, thermal analysis and luminescence techniques. *Archaeological and Anthropological Sciences*, *10*(4), 849–864. https://doi.org/10.1007/s12520-016-0409-x

Savitzky, A., & Golay, M. J. E. (1964). Smoothing and differentiation of data by simplified least squares procedures. *Analytical Chemistry*, *36*(8), 1627–1639. https://doi.org/10.1021/ac60214a047

Semiz, B., Abay, E., Dedeoğlu, F., Konakçi, E., & Ozan, A. (2018). An archaeometric investigation of early and middle bronze age pottery from the upper meander basin in southwestern Anatolia. *Mediterranean Archaeology and Archaeometry*, *18*(3), 121–150.

Shoval, S. (2003). Using FT-IR spectroscopy for study of calcareous ancient ceramics. *Optical Materials*, *24*(1), 117–122. https://doi.org/10.1016/S0925-3467(03)00114-9

Shoval, S. (2016). Fourier transform infrared spectroscopy (FT-IR) in archaeological ceramic analysis.

Shoval, S., Gaft, M., Beck, P., & Kirsh, Y. (1993). Thermal behaviour of limestone and monocrystalline calcite tempers during firing and their use in ancient vessels. *Journal of Thermal Analysis*, *40*(1), 263–273. https://doi.org/10.1007/BF02546577

Shoval, S., & Paz, Y. (2015). Analyzing the fired-clay ceramic of EBA Canaanite pottery using FT-IR spectroscopy and LA-ICP-MS. *Periodico di Mineralogia*, *84*, 213–231.

Shoval, S., Yadin, E., & Panczer, G. (2011). Analysis of thermal phases in calcareous iron age pottery using FT-IR and Raman spectroscopy. *Journal of Thermal Analysis and Calorimetry*, *104*(2), 515–525. https://doi.org/10.1007/s10973-011-1518-5

Tanasi, D., Caso, G., Tykot, R. H., & Amoroso, D. (2019). Petrographic and chemical characterization of middle bronze age pottery from Sicily: Towards a definition of an Etnean production. *Rendiconti Lincei-Scienze Fisiche E Naturali*, *30*(2), 399–415. https://doi.org/10.1007/s12210-019-00803-x

Tarhan, İ., Işık, İ., & Söğüt, B. (2021). Application of ATR-FTIR spectroscopy in tandem with chemometrics for assessing the firing conditions of Hellenistic and Roman ceramic shards excavated from the ancient city of Stratonikeia in South-Western Turkey. *Microchemical Journal*, *162*, 105852. https://doi.org/10.1016/j.microc.2020.105852

Tarte, P. (1963). Etude infra-rouge des orthosilicates et des orthogermanates—II: Structures du type olivine et monticellite. *Spectrochimica Acta*, *19*(1), 25–47. https://doi.org/10.1016/0371-1951(63)80092-2

Tuna, Y., Massa, M., & Şahin, F. (2022). The Konya Basin metallic ware: A typological, technological and chronological examination of a distinctive early bronze age ware. *Oxford Journal of Archaeology*. (PMID: in press).

Türkteki, M. (2014). Early bronze age pottery-manufacture in Western Anatolia: Identifying hybrid technologies through X-ray analysis. *Anatolica*, *40*, 93–109.

Ünlü, E. (2009). *Technological and stylistic evaluation of the early bronze age Pottery at Tarsus-Gozlukule, Turkey: Pottery production and its interaction with economic, social, and cultural spheres*. University of Pennsylvania.

Velraj, G., Tamilarasu, S., & Ramya, R. (2015). FTIR, XRD and SEM-EDS studies of archaeological pottery samples from recently excavated site in Tamil Nadu, India. *Materials Today: Proceedings*, *2*(3), 934–942.

Yener, A. K. (2000). *The domestication of metals: The rise of complex metal industries in Anatolia: Culture and history in the ancient near east* (Vol. 4). Brill. https://doi.org/10.1163/9789004496934

Yu, R. S., Ito, K., Hirata, K., Sato, K., Zheng, W., & Kobayashi, Y. (2003). Positron annihilation study of defects and Si nanoprecipitation in sputter-deposited silicon oxide films. *Chemical Physics Letters*, *379*(3–4), 359–363. https://doi.org/10.1016/j.cplett.2003.08.056

SUPPORTING INFORMATION

Additional supporting information can be found online in the Supporting Information section at the end of this article.

How to cite this article: Tarhan, İ., Massa, M., Tuna, Y., & Şahin, F. (2023). An archaeometric study of the Konya basin metallic ware through FTIR and XRD analysis with chemometrics: Central Anatolian Early Bronze Age ceramics. *Archaeometry*, *65*(1), 136–150. https://doi.org/10.1111/arcm.12812